Lyapunov Function and Sliding Mode Control Approach for the Solar-PV Grid Interface System

Miloud Rezkallah, *Member, IEEE*, Shailendra Kumar Sharma, *Senior Member, IEEE*, Ambrish Chandra, *Fellow, IEEE*, Bhim Singh, *Fellow, IEEE*, and Daniel R. Rousse

***Abstract*—This paper deals with control of a solar-photovoltaic (PV) power-generating system interfaced with the grid. A sliding mode control approach is used for achieving maximum power tracking control of a solar-PV array. The Lyapunov function-based control approach is designed and modeled for the dc–ac inverter to serve the functions of an active power injection to the grid, balanced grid currents at unity power factor and load currents harmonics compensation. The proposed approaches eliminate the need of adjustment of system parameters under changing loads and generation scenario. The effectiveness of the proposed control strategies is established using its stability analyses. The performance of the solar-PV power-generating system with the proposed control algorithms is demonstrated using simulation and experimental studies under various operating conditions.**

***Index Terms*—Lyapunov-based function, maximum power tracking (MPT), photovoltaic (PV) array, power quality (PQ) improvement sliding mode control (SMC) approach, stability analysis.**

I. Introduction

RENEWABLE energy programs are receiving reasonable attention worldwide to cater the needs of electricity. According to U.S. Energy Information Administration reports, the growth rate of such programs is 2.5% per/year [1]. In fact, there is tremendous potential available to produce electricity using the solar energy. The recent trends are indicating increase in capital investments of solar-based power projects. Solar photovoltaic (PV) panel generates dc power and hence additional components, such as power converters, are instrumental to tie it with the ac grid. Further, solar-based power generation is intermittent in nature which varies very rapidly changes in solar irradiation. Therefore, solar-based power penetration into grid adversely affects the stability of the network and quality of supply. For the secure and reliable integrations of such solar-PV systems with the grid, different standards are in practice in various countries such as in [2]. To control the operation under these guidelines, solutions have also been reported in the literature using a single-stage inverter [3], [4] and two-stage inverter [5]–[8].

To know which topology is preferred for a typical application, a comparative study has been made in [9]. The single-stage topology is considered more efficient due to less number of components. However, two-stage power conversion provides more flexibility in design, operation, and control. The dc–dc converter is employed in between the solar-PV array and dc link of an inverter and controlled to achieve maximum power tracking (MPT) from a solar-PV array.

Various control approaches have been reported in the literature to improve the efficiency of the solar-PV array [10]. Each MPT method has its own advantages and disadvantages. Compared to the existing MPT methods, the perturbation and observation method is widely used in industry due to its simplicity, but it suffers during rapid solar irradiation change [10], [11]. In addition, at steady state, the operating point oscillates around the maximum power point (MPP), which leads in losing some amount of the available energy, increased switching noise and losses. Many solutions have been reported in the literature to solve this problem. In [12], it has been proposed to reduce steps size. This technique is effective but it makes the control sluggish during rapid change in solar irradiation. In [13], adaptive perturbation step size has been employed to get better performance. However, this method is complex in implementation as it needs the location of the operating point. In addition, the control is switched in between adaptive duty cycle and fixed duty cycle control, which makes its implementation difficult in real time.

Sliding mode approach (SMC) as solution is proposed in [14] to solve the problem related to the operating point that oscillates around the MPP, and to ensure stability of the system with fast dynamic response. However, chattering phenomenon is its major drawback and because of it, this induces many undesirable oscillations in control signal. Therefore, to maintain the amplitude of oscillation at low level, chattering must be decreased or eliminated. To achieve this objective, many chattering suppression methods have been suggested in the literature. In [15] and [16], boundary layer solution is proposed, and in [17], observer-based solution is used. Furthermore, in [18], sliding mode is limited to an inner control loop of a cascaded control structure to reduce the chattering, and in [19]–[23], generating integral

Manuscript received October 26, 2015; revised February 17, 2016 and May 4, 2016; accepted June 14, 2016. Date of publication September 8, 2016; date of current version December 9, 2016. This work was supported in part by the Fonds de Recherche du Québec–Nature et Technologies.

M. Rezkallah and A. Chandra are with the Electrical Engineering Department, École de Technologie Supérieure, Montréal, QC H3C1K3, Canada (e-mail: mrezkallah73@gmail.com; ambrish.chandra@etsmtl.ca).

S. K. Sharma is with the Electrical Engineering Department, Shri Govindram Seksaria Institute of Technology and Science, Indore 452003, India (e-mail: ssharma.iitd@gmail.com).

B. Singh is with the Electrical Engineering Department, Indian Institute of Technology Delhi, New Delhi 110016, India (e-mail: bsingh@ee.iitd.ac.in).

D. R. Rousse is with the Mechanical Engineering Department, École de Technologie Supérieure, Montréal, QC H3C1K3, Canada (e-mail: daniel.rousse@etsmtl.ca).

Color versions of one or more of the figures in this paper are available online at http://ieeexplore.ieee.org.

Digital Object Identifier 10.1109/TIE.2016.2607162

0278-0046 © 2016 IEEE. Personal use is permitted, but republication/redistribution requires IEEE permission.
See http://www.ieee.org/publications_standards/publications/rights/index.html for more information.

sliding mode, terminal SMC, and nonsingular terminal SMC have been proposed.

Each proposed technique has its own advantages and disadvantages, but it is clear that the selection criterion of solution, which is able to eliminate the chattering phenomenon, is related to the order of the mathematical model of the uncertain system and the type of application. Nevertheless, in some applications, such as aircraft and electric automotive control, which require a high level of precision, advanced SMC is strongly advocated. Unfortunately, their implementations in real time are challenging. However, in other typical applications, SMC is applied to the control of the dc–dc converters or dc–ac inverters. In such applications, a conventional nonlinear SMC is considered more suitable as they are less complex and easy to implement in real time [24].

Improved nonlinear SMC to drive the PV voltage to follow its reference is proposed in [25]. This approach is simple, but unfortunately the use of the low-pass filter between the perturb and observe controller and the SMC influences the dynamic response of the system. Further, the use of sensed capacitor current in the model reduces the reliability particularly in high environmental temperature conditions.

For improving the grid stability and power quality (PQ) at the point of common coupling (PCC) and delivering the generated power from the PV array in to the grid, the dc–ac inverter is mostly employed. Several control schemes have been reported in the literature to achieve above tasks using the dc–ac inverter, such as model predictive control and instantaneous PQ control [26]. Some control approaches have used adaptive algorithms such as presented in [27] and [28]. However, most of these approaches have not extensively verified under the presence of nonlinear loads with grid supply. In addition, they have employed more number of proportional-integral (PI) controllers, due to which steady-state error at the fundamental frequency cannot be nullified in the presence of dynamics of the integral action.

Lyapunov function-based control for a shunt hybrid active filter is proposed in [29] to improve the PQ at the PCC. Compared to the other control approaches, the Lyapunov function-based control is robust and effective because of the use of less PI controllers and stability enhancement. Unfortunately, authors have not considered all system parameters in selection of the gain controller, which leads that the proposed approach may suffer during transition period. To overcome this drawback, the authors in [30] have enhanced this control approach by integrating new outer voltage loop in order to eliminate the steady-state error in the output voltage during perturbation or transition period. This approach is effective but it cannot be used for a three-phase inverter.

Inspired from the previous work, this paper presents sliding mode-based layer concept and Lyapunov function approach used for the control of the dc–dc boost converter and the dc–ac inverter, respectively. The proposed approach eliminates the application of many PI controllers for the control and uses only single PI controller for dc-link voltage regulation. The detail modeling, design of the gain controllers, and stability analysis of the proposed approach are investigated to prove its efficacy under various field operating conditions. Simulation and experimental results are presented subsequently in the presence of different loads and change in solar irradiations.

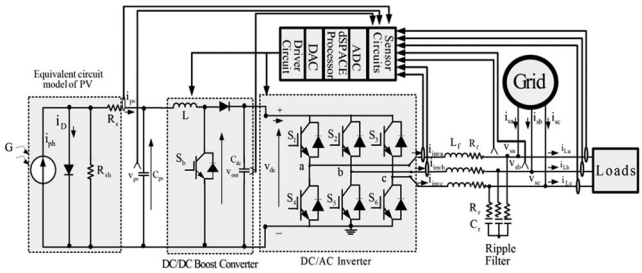

Fig. 1. Schematic diagram of the solar-PV power-generation system.

II. System Configuration

Fig. 1 shows the proposed system under study. It consists of a solar-PV array tied to the grid through a dc–dc boost converter and a three-phase dc–ac inverter. To attenuate the switching ripples at the ac terminals of the dc–ac inverter, a star-connected three terminal *RC* ripple filter is connected. The dc–dc boost converter is controlled using the SMC approach in order to achieve MPT from the PV array with regulating the dc-link voltage of the PV array. The dc–ac inverter is controlled using the Lyapunov function-based approach in order to feed the solar-PV-generated power to the grid, to compensate harmonics present in load currents and to ensure balanced grid currents at unity power factor.

III. Modeling and Control of Converters

Modeling, control, and stability analysis of the dc–dc boost converter and the dc–ac inverter are presented as follows.

A. Modeling and Design of Control Scheme for the DC–DC Boost Converter

The objectives of the proposed control for the dc–dc boost converter are to achieve the MPT from the solar-PV array and step up its output voltage. To achieve these tasks, the PV output current $i_{\rm pv}$ and voltage $v_{\rm pv}$, as well as the output voltage of the boost converter $v_{\rm out}$, which represents the dc-bus voltage $v_{\rm dc}$ are sensed. The control provides the duty cycle u required for switching the control switch.

The model of boost converter is obtained based on two operating modes in continuous conduction as follows:
For $S_b = 1$ (ON)

$$L\left(\partial i_L/\partial t\right) = v_{\rm pv} \tag{1}$$

$$C_{\rm dc}\left(\partial v_{\rm dc}/\partial t\right) = -\left(v_{\rm dc}/R\right). \tag{2}$$

For $S_b = 0$ (OFF)

$$L\left(\partial i_L/\partial t\right) = v_{\rm pv} - v_{\rm dc} \tag{3}$$

$$C_{\rm out}\left(\partial v_{\rm dc}/\partial t\right) = i_L - \left(v_{\rm dc}/R\right) \tag{4}$$

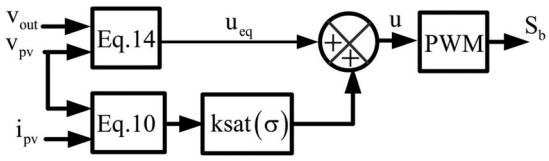

Fig. 2. Scheme for control of the dc–dc boost converter.

where L, C_{out}, and R represent inductance, capacitance of the filter, and the equivalent load resistance for the boost converter, respectively.

Based on (1) to (4), the state-space average model of dc–dc boost converter are obtained as follows:

$$(\partial i_L/\partial t) = (v_{\text{pv}}/L) - (1-u)(v_{\text{dc}}/L) \tag{5}$$

$$(\partial v_{\text{dc}}/\partial t) = (1/C_{\text{out}})[(i_L(1-u)) - (v_{\text{dc}}/R)] \tag{6}$$

where u is the duty cycle.

B. MPT Control Based on the SMC

The MPT is achieved using the SMC. Fig. 2 shows the block diagram of the proposed SMC based control of dc–dc converter. The design is obtained using the following steps.

1) Selecting of Sliding Surface: The sliding surface σ is selected as given in (7), to ensure reaching the surface and extracting the maximum power from the solar-PV array

$$\sigma = (\partial P_{\text{pv}}/\partial i_{\text{pv}}) = 0 \tag{7}$$

where P_{pv} is the PV output power, which is defined as follows:

$$P_{\text{pv}} = v_{\text{pv}} i_{\text{pv}}. \tag{8}$$

Substituting (8) in (7), the following expression is obtained as follows:

$$\sigma = (\partial P_{\text{pv}}/\partial i_{\text{pv}}) = \partial(v_{\text{pv}} i_{\text{pv}})/\partial i_{\text{pv}}. \tag{9}$$

Rearranging (9), the sliding surface is defined as follows:

$$\sigma = v_{\text{pv}} + i_{\text{pv}}(\partial v_{\text{pv}}/\partial i_{\text{pv}}). \tag{10}$$

2) Equivalent Criteria for Control: The equivalent control is obtained by setting the derivative of (10) to 0. So, the structure of the desired control is defined as follows:

$$u = u_{\text{eq}} + k\,\text{sign}\,(\sigma) \tag{11}$$

where k is a gain constant and u_{eq} is the equivalent control, which is obtained as follows:

$$\begin{aligned}(\partial\sigma/\partial t) &= (\partial\sigma/\partial i_L)(\partial i_L/\partial t)\\ &= (\partial\sigma/\partial i_L)[(v_{\text{pv}}/L) - (1-u)(v_{\text{dc}}/L)].\end{aligned} \tag{12}$$

The nontrivial solution of (12) is given as follows:

$$v_{\text{pv}} - (1-u)v_{\text{dc}} = 0. \tag{13}$$

From (13), the following equivalent control is obtained:

$$u_{\text{eq}} = 1 - (v_{\text{pv}}/v_{\text{dc}}). \tag{14}$$

The duty cycle u is limited between 0 and 1. Therefore, the structure of SMC is defined as follows:

$$u = \begin{cases} 1 & \text{if } u_{\text{eq}} + k\,\text{sign}\,(\sigma) \geq 0 \\ 0 & \text{if } u_{\text{eq}} + k\,\text{sign}\,(\sigma) \leq 0. \end{cases} \tag{15}$$

3) Stability Analysis: The objective of the approach using SMC is to ensure the convergence of the operating points to define the sliding boundary. Therefore, for assuring the stability of the control, Lyapunov function is used as follows:

$$V = (1/2)\sigma^2. \tag{16}$$

The system is considered globally stable if the derivative of (16) is negative

$$(\partial V/\partial t) = \sigma(\partial\sigma/\partial t) \langle 0. \tag{17}$$

Substituting (5) and (10) in (17), the following relationship, which is composed of three terms, is obtained:

$$\overbrace{(v_{\text{pv}} + i_L(\partial v_{\text{pv}}/\partial i_L))}^{\text{Term1}}\overbrace{(2(\partial v_{\text{pv}}/\partial i_L) + i_L(\partial^2 v_{\text{pv}}/\partial^2 i_L))}^{\text{Term2}}\overbrace{((v_{\text{pv}}/L) - (1-u)(v_{\text{dc}}/L))}^{\text{Term3}}\langle 0 \tag{18}$$

where v_{pv} is the PV output voltage, and it is defined as follows [19]:

$$v_{\text{pv}} = (k_b T A/q)\ln((i_{\text{ph}} + i_D - i_L)/i_D). \tag{19}$$

The PV saturation current (i_D) and the light-generated current (i_{ph}) are expressed as follows:

$$i_D = i_{\text{rr}}(T/T_r)^3 EXP[((qE_g)/(KQA))((1/T_r) - (1/T))] \tag{20}$$

$$i_{\text{ph}} = G[i_{\text{scr}} + k_i(T - T_r)] \tag{21}$$

where $k_b, T, A, q, G, i_{\text{scr}}, T_r, k_i, i_{\text{rr}}, E_g$, and Q represent the Boltzmann's constant, cell temperature, ideality factor, charge of an electron, solar irradiance, short-circuit current, reference temperature, short-circuit temperature coefficient, saturation current, band-gap energy of the material and total electron charge, respectively.

The terms in (18) contain the derivative and the second derivative of (19), which are given as follows:

$$(\partial v_{\text{pv}}/\partial i_L) = -\overbrace{(k_b T A/q)}^{\text{Term1}}\overbrace{(i_D/(i_{\text{ph}} + i_D - i_L))}^{\text{Term2}} \tag{22}$$

$$(\partial^2 v_{\text{pv}}/\partial^2 i_L) = -\overbrace{(k_b T A/q)}^{\text{Term1}}\overbrace{\left(i_D/(i_{\text{ph}} + i_D - i_L)^2\right)}^{\text{Term2}}. \tag{23}$$

In order to verify that the system is globally stable, the sign of the (18) is obtained. It is observed that (18) contains three terms. The first and the second terms contain the first derivative and the second derivative of the output PV voltage given in (22) and (23), respectively. However, to obtain the sign of (18), it is better to verify the sign of each term in this expression independently. With help of the parameters of the PV array given in Table II in

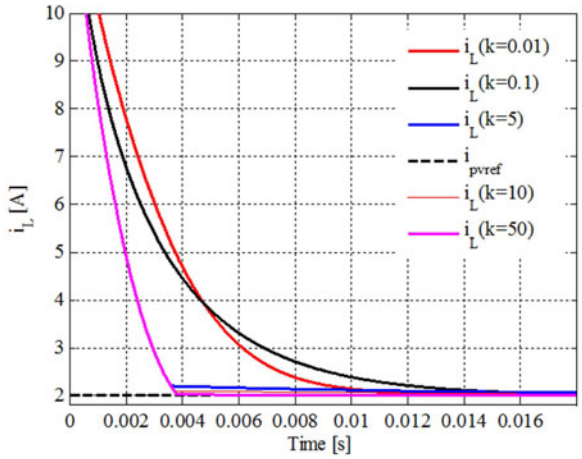

Fig. 3. Dynamic response of inductor current for different gain control values.

the Appendix [19], the first term of (22) is calculated equal to $k_b TA/q = 0.0026$. In addition, as it is observed in the equivalent model of the PV array shown in Fig. 1 that the current $i_{\rm ph}$ is always greater than currents i_D and i_L. Therefore, the second term in (22) is always less than the first one. Based on above, the sign of (22) is always negative.

The same logic is applied to determine the sign of the second derivative of the output voltage given in (23). In comparison with (22), the denominator of the second term in (23) is square; it leads that second term is smaller than the first term ($k_b TA/q = 0.0026$). Therefore, the sign of (23) is also negative. Based on these results, it is concluded that the sign of the second term of (18) is negative.

The sign of the first term in (18) is positive because of the value of the output PV voltage is positive and greater to $(i_L(\partial v_{\rm pv}/\partial_{\rm iL}))$. Further, the sign of the third term in (18) must be positive. To verify the sign of third term in (18), one replaces *d* in the third termby (11) and (14). After rearranging and simplifying the third term, following expression is obtained as follows:

$$\left(\overbrace{(v_{\rm dc}/L)}^{\rm Term1}\ \overbrace{ksgn(\sigma)}^{\rm Term2}\right)\rangle 0. \tag{24}$$

The first term is always positive. Therefore, to satisfy the condition given in (18), the second term in (24) should be positive, which is obtained by applying the following conditions:

$$\begin{cases} \text{if} \quad \text{sign}(\sigma)\langle 0\,, & k\langle -1 \\ \text{if} \quad \text{sign}(\sigma)\rangle 0\,, & k\rangle 1 \end{cases} \tag{25}$$

where *k* is positive gain parameter.

Based on the previous discussion, it is verified that proposed control approach is stable for the dc–dc boost converter.

The chattering phenomenon caused by the continuous jumping of the system trajectory when it is operating near sliding surface ($\sigma = 0$) is the major drawbacks of the proposed SMC approach given in (15). Therefore, to eliminate this undesired

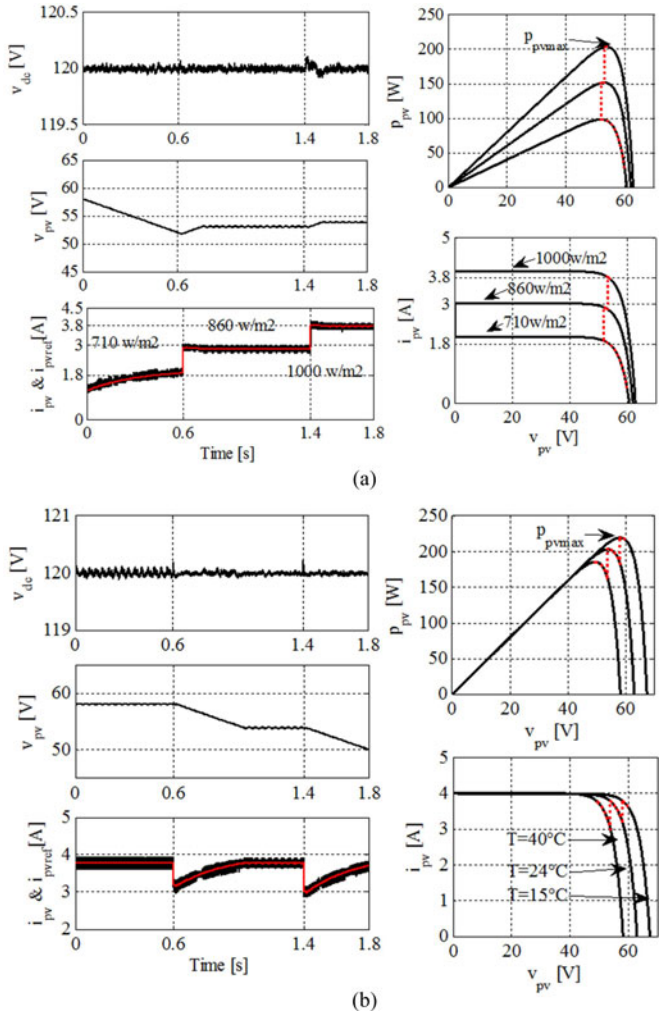

Fig. 4. Simulation results of the dc-link voltage $v_{\rm dc}$, output PV voltage and current, $i_{\rm pv} = f(v_{\rm pv})$ and $p_{\rm pv} = f(v_{\rm pv})$ at: (a) fixed temperature and different solar irradiation, and (b) at fixed solar irradiation and different temperature.

chattering phenomenon, sliding layer concept is used as shown in Fig. 2 and described as follows:

$$\text{sat}(\sigma, \Phi) \begin{cases} 1, & \sigma \succ \Phi \\ \sigma/\Phi, & |\sigma| \le \Phi \\ -1, & \sigma \prec -\Phi \end{cases} \tag{26}$$

or

$$\text{sat}(\sigma, \Phi) = \begin{cases} \text{sign}(\sigma)\,, & |\sigma| \succ \Phi \\ \sigma/\Phi, & |\sigma| \le \Phi \end{cases} \tag{27}$$

where Φ represents the sliding layer, which is defined between –0.5 and 0.5.

4) Controller Gain Design: To ensure that the proposed SMC performs better, the control gain (*k*) should be selected to drive the trajectory to the slide surface in infinite time. The dynamic response of the inductor current, which represents the output PV current for different values of "*k*," is shown in Fig. 3. It is observed that for high values of *k*, the dynamic

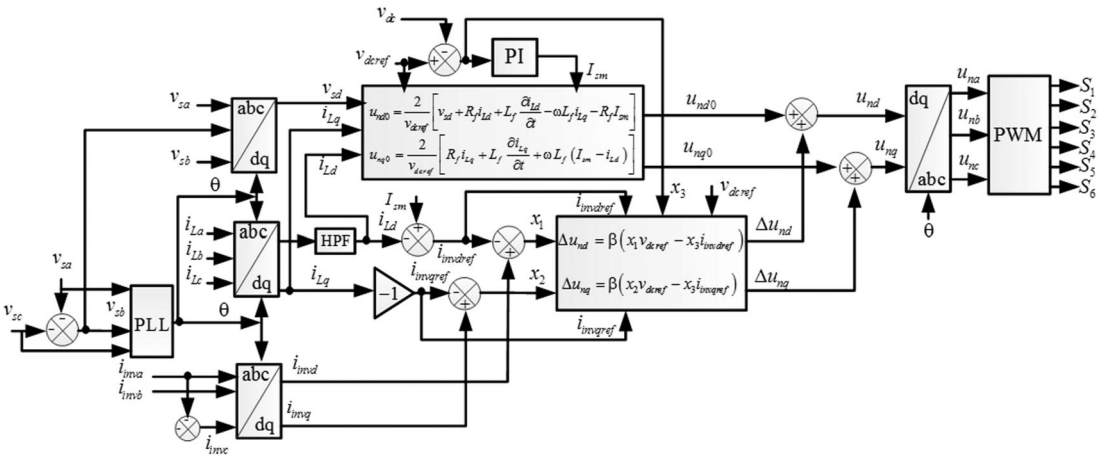

Fig. 5. Control algorithm of the dc–ac inverter.

response of the inductor current is faster. Therefore, for fast dynamic response, the control gain is selected equal to $k = 50$.

Testing of the performance of the proposed SMC using the optimal value of k is shown in Fig. 4. The simulations are carried out using MATLAB/Simulink. Observations are obtained at fixed temperature ($T = 24\,^{\circ}\mathrm{C}$) and different solar irradiations as shown in Fig. 4(a), and at different temperatures with fixed solar irradiations ($G = 1000\ \mathrm{w/m^2}$), as shown in Fig. 4(b). The output PV current ($i_{\mathrm{pv}} = {}_{\mathrm{iL}}$) follows its desired reference at finite time and the output PV voltage ($v_{\mathrm{dc}} = v_{\mathrm{out}}$) is maintained constant during both tests, which confirm that the proposed SMC performs better at this optimal value of control gain.

C. MPT Control Based on the SMC

The block diagram of the proposed Lyapunov-based control algorithm for the dc–ac inverter is shown in Fig. 5. The inverter is switched to control the active power flow between the dc bus and the grid, to improve the PQ at the PCC by compensating load current harmonics and to balance the grid currents at unity power factor. For the control scheme, load currents, inverter currents, and grid voltages are sensed.

The control laws u_{na}, u_{nb}, and u_{nc} are determined using these sensed signals. Park's transformation is used to obtain synchronously rotating d–q variables for load currents, inverter currents, and grid voltages. The phase-locked loop is used to calculate the grid voltage phase angle used for the transformation. The control laws are obtained using mathematical modeling of the dc–ac inverter, control design and after verification using stability analysis.

The mathematical expressions used for the modeling are as follows. Applying Kirchhoff laws at inverter ac and dc terminals provides expression for three-phase supply system, which are transferred into synchronous rotating grid voltage reference frame using Park's transformation. The resulting mathematical model in d–q reference frame is expressed as follows:

$$\begin{cases} (\partial i_{\mathrm{invd}}/\partial t) = -(R_f/L_f)\, i_{\mathrm{invd}} + \omega i_{\mathrm{invq}} - (u_{\mathrm{nd}}/2L_f)\, v_{\mathrm{dc}} \\ \qquad\qquad + (v_{\mathrm{sd}}/L_f) \\ (\partial i_{\mathrm{invq}}/\partial t) = -(R_f/L_f)\, i_{\mathrm{invq}} - \omega i_{\mathrm{invd}} - (u_{\mathrm{nq}}/2L_f)\, v_{\mathrm{dc}} \\ \qquad\qquad + (v_{\mathrm{sq}}/L_f) \\ (\partial v_{\mathrm{dc}}/\partial t) = (3/4)\left((u_{\mathrm{nd}}/C_{\mathrm{dc}})\, i_{\mathrm{invd}} + (u_{\mathrm{nq}}/C_{\mathrm{dc}})\, i_{\mathrm{invq}}\right) \end{cases} \tag{28}$$

where R_f, L_f, C_{dc}, i_{invd}, i_{invq}, v_{sd}, v_{dc}, ω, u_{nd}, and u_{nq} denote the equivalent resistance and inductance at the ac terminals of dc–ac inverter, dc-link capacitor of the dc bus, inverter currents in d–q frame, equivalent voltage in d frame, dc voltage, angular frequency of the grid, and the control laws in d–q reference frame, respectively.

For the unity power factor operation of grid currents, the reference q-axis component of grid currents i_{sq} must be kept equal to zero. Moreover, the q-axis component of the grid voltage is considered equal to zero ($v_{\mathrm{sq}} = 0$) for reference frame aligned with voltage vector. Therefore, under the steady-state conditions, following equality conditions are justified:

$$v_{\mathrm{dc}} = v_{\mathrm{dcref}}, i_{\mathrm{sd}} = I_{\mathrm{sm}}, i_{\mathrm{sq}} = 0, u_{\mathrm{nd}} = u_{\mathrm{nd0}}, u_{\mathrm{nq}} = u_{\mathrm{nq0}},$$
$$i_{\mathrm{invd}} = i_{\mathrm{invdref}} = I_{\mathrm{sm}} - i_{\mathrm{Ld}}, i_{\mathrm{invq}} = i_{\mathrm{invqref}} = -i_{\mathrm{Lq}}$$

where I_{sm}, i_{invdref}, i_{invqref}, u_{nd0}, and u_{nq0} denote the amplitude of the grid current, d–q axis inverter reference currents, and the d–q axis steady-state value of the control variables.

Putting these equalities in (28), the following expressions are obtained as follows:

$$\begin{cases} u_{\mathrm{nd0}} = (2/v_{\mathrm{dcref}})\left[v_{\mathrm{sd}} + R_f i_{\mathrm{Ld}} + L_f\,(\partial i_{\mathrm{Ld}}/\partial t)\right. \\ \qquad\qquad \left. - \omega L_f i_{\mathrm{Lq}} - R_f I_{\mathrm{sm}}\right] \\ u_{\mathrm{nq0}} = (2/v_{\mathrm{dcref}})\left[R_f i_{\mathrm{Lq}} + L_f\,(\partial i_{\mathrm{Lq}}/\partial t) + \omega L_f\right. \\ \qquad\qquad \left. \times\ (I_{\mathrm{sm}} - i_{\mathrm{Ld}})\right] \end{cases} \tag{29}$$

and

$$\begin{cases} u_{\mathrm{nd}} = u_{\mathrm{nd0}} + \Delta u_{\mathrm{nd}} \\ u_{\mathrm{nq}} = u_{\mathrm{nq_0}} + \Delta u_{\mathrm{nq}} \end{cases} \tag{30}$$

where Δu_{nd} and Δu_{nq} denote perturbations of global switching functions.

1) Stability Analysis: The stability of the proposed control system is verified using Lyapunov stability criterion, which is presented in Section III (B_3). The system under consideration is stable if the total energy of the dc–ac inverter system decreases along the system trajectories. The positive-definite Lyapunov function in this case is described as follows:

$$V = (3/2)\, L_f x_1^2 + (3/2)\, L_f x_2^2 + (1/2)\, C_{\mathrm{dc}} x_3^2. \tag{31}$$

Thus, the system is considered stable if the derivative of (31) is negative

$$(\partial V/\partial t) = \left(\partial \left((3/2)\, L_f x_1^2 + (3/2)\, L_f x_2^2 + (1/2)\, C_{\mathrm{dc}} x_3^2\right)/\partial t\right) \langle 0. \tag{32}$$

Rearrangement of (32) gives

$$(\partial V/\partial t) = 3L_f x_1\, (\partial x_1/\partial t) + 3L_f x_2\, (\partial x_2/\partial t) + C_{\mathrm{dc}} x_3\, (\partial x_3/\partial t)\, \langle 0. \tag{33}$$

Considering

$$x_1 = (i_{\mathrm{invd}} - i_{\mathrm{invdref}}),\ x_2 = (i_{\mathrm{invq}} - i_{\mathrm{invqref}}),$$
$$x_3 = (v_{\mathrm{dc}} - v_{\mathrm{dcref}}). \tag{34}$$

Substituting (30) and (32) in (28), and with help of (29), the following expressions are obtained as follows:

$$(\partial x_1/\partial t) = -(R_f/L_f)\, x_1 + \omega x_2 - ((u_{\mathrm{nd0}} + \Delta u_{\mathrm{nd}})/L_f)\, x_3 + (v_{\mathrm{sd}}/L_f) \tag{35}$$

$$(\partial x_2/\partial t) = -(R_f/L_f)\, x_2 - \omega x_1 - ((u_{\mathrm{nq0}} + \Delta u_{\mathrm{nq}})/L_f)\, x_3 \tag{36}$$

$$(\partial x_3/\partial t) = (3/4)\left(\begin{array}{l}((u_{\mathrm{nd0}} + \Delta u_{\mathrm{nd}})/C_{\mathrm{dc}})\, (x_1 + i_{\mathrm{nvdref}}) + \\ ((u_{\mathrm{nq0}} + \Delta u_{\mathrm{nq}})/C_{\mathrm{dc}})\, (x_2 + i_{\mathrm{nvqref}})\end{array}\right). \tag{37}$$

Substituting (35)–(37) into (34) gives the following expression:

$$(\partial V/\partial t) = \overbrace{-3R_f(x_1^2 + x_2^2)}^{\text{Term 1}} - \overbrace{(3/2)\, (x_1 v_{\mathrm{dcref}} - x_3 i_{\mathrm{invdref}})\, \Delta u_{\mathrm{nd}}}^{\text{Term 2}} - \overbrace{(3/2)\, (x_2 v_{\mathrm{dcref}} - x_3 i_{\mathrm{invqref}})\, \Delta u_{\mathrm{nq}}}^{\text{Term 3}}. \tag{38}$$

It is observed that the first term $\overbrace{-3R_f(x_1^2 + x_2^2)}^{\text{Term 1}}$ is always negative. Therefore, to verify the Lyapunov stability condition, the second and the third terms should be negative. To obtain this negative sign, the perturbations of the global switching (Δu_{nd} and Δu_{nq}) should be chosen as follows:

$$\Delta u_{\mathrm{nd}} = \beta\, (x_1 v_{\mathrm{dcref}} - x_3 i_{\mathrm{invdref}}), \quad \beta \rangle 0 \tag{39}$$

$$\Delta u_{\mathrm{nq}} = \beta\, (x_2 v_{\mathrm{dcref}} - x_3 i_{\mathrm{invqref}}), \quad \beta \rangle 0 \tag{40}$$

where β denotes the gain of the controller.

TABLE I
CHOICE OF β

β	Time response (s)	THD at the PCC (%)
0.1	0.2	8.10
0.5	0.165	4.16
1	0.16	3.68
2.5	0.16	3.5
5	0.16	3.4
10	0.16	6.72
20	0.16	6.79

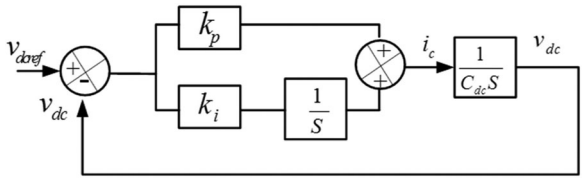

Fig. 6. Transfer function of the dc-link voltage regulation.

2) Choice of β: The choice of β is based on the dynamic response of the system and desired PQ at the PCC. However, the correct value of β corresponds to fast dynamic response of the system and less harmonic distortion (total harmonic distortion (THD)) of grid current at the PCC. In order to achieve these objectives, several cases with different β are considered as given in Table I. It is observed that with $\beta = 5$, the response of the system is fast ($t = 0.16$ s) and the THD grid current is least (3.4%). Therefore, β is considered 5 for obtaining the control.

3) DC Voltage Regulation: The dc-link voltage v_{dc} must be maintained constant at the reference value to ensure correct injection of the power to the grid under change in solar irradiance and to improve the PQ at the PCC. As shown in Fig. 6, a conventional PI controller is adopted to regulate the dc-link voltage.

The output of PI controller in the time domain is given as follows:

$$i_c(t) = k_p \Delta v_{\mathrm{dc}}(t) + k_i \int \Delta v_{\mathrm{dc}}(t) dt \tag{41}$$

where k_p, k_i, $i_c\,(t)$, and $\Delta v_{\mathrm{dc}}\,(t)$ denote the proportional and integral coefficients, link active power component of grid current, and the dc-link voltage error, respectively.

The transfer function of a PI controller is found by taking the Laplace transform of equation given in (41) as follows:

$$G(s) = k_p + (k_i/s). \tag{42}$$

The open-loop transfer function of the dc-link voltage regulation loop shown in Fig. 6 is described as follows:

$$G(s) = (k_p + (k_i/s))\, (1/(C_{\mathrm{dc}} s)) \tag{43}$$

and the corresponding closed-loop transfer function is expressed as follows:

$$H(s) = (1/C_{\mathrm{dc}})\left((k_p s + k_i)/\left(s^2 + (k_p/C_{\mathrm{dc}})\, s + (k_i/C_{\mathrm{dc}})\right)\right). \tag{44}$$

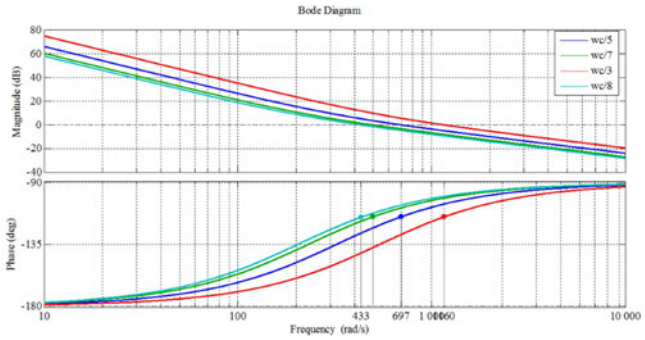

Fig. 7. Bode diagram for the open-loop transfer function of the dc-link voltage regulation.

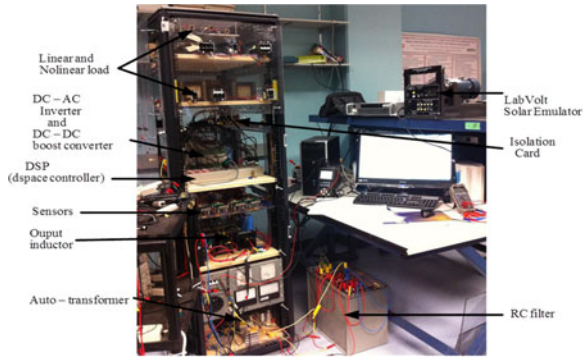

Fig. 8. Photograph of the experimental system.

The closed-loop function *H(S)* is the second-order system, in which the damping ratios ξ and the system bandwidth ω_c are equal to

$$\begin{cases} 2\xi\omega_c = (k_p/C_{\rm dc}) \Rightarrow k_p = 2C_{\rm dc}\xi\omega_c \\ \omega_c^2 = (k_i/C_{\rm dc}) \Rightarrow k_i = C_{\rm dc}\omega_c^2. \end{cases} \tag{45}$$

To achieve a good compromise between dynamic and static performances, the value of damping ratios ξ must lie between 0.4 and 0.8. The bandwidth frequency that gives phase margin varies between 45° to 65°. Bode plot based on different values of the bandwidth frequency is used as shown in Fig. 7. It is observed that for fast and stable response, the bandwidth frequency is equal to 433 rad/s and the phase margin is equal to 64°. The k_p and k_i corresponding to the selected bandwidth frequency are 0.98 and 200, respectively.

4) Selecting of DC-Link Voltage: The minimum dc-link voltage of the voltage-source converter should be greater than twice the peak of the ac phase voltage of the grid. The dc-link voltage $V_{\rm dc}$ is estimated as follows [31]:

$$V_{\rm dc} \geq v_{\rm sab}((2\sqrt{2})/(\sqrt{3}m)) \tag{46}$$

where $V_{\rm dc}$, m, and $v_{\rm sab}$ denote the minimum value of the dc-link voltage, modulation index, which is considered as 1, and the ac phase voltage of the grid, respectively. Hence, the minimum dc-link voltage from (42) is estimated as 81.64 V, and is selected as 120 V.

IV. Simulation and Experimental Results

The performance of the solar-PV power generation system as shown in Fig. 1 and its proposed control algorithm presented in Figs. 2 and 5 are verified using the simulation model developed in MATLAB/Simulink. A prototype of the system is developed in the laboratory as shown in Fig. 8. The performance is evaluated on a small-scale 500 VA system using a DSP (dSPACE) controller; LabVolt solar emulator is used as a PV array. Hall's effect current sensors (LEM LA-55P), Hall's effect voltage sensors (LEM LV-25P), signal conditioning circuit, three-leg ready on shelf inverter, and dc–dc boost converter are used for prototype development. The gating signals for converters are obtained using three-phase and single-phase pulse width modulation blocks of DSP and an isolation card.

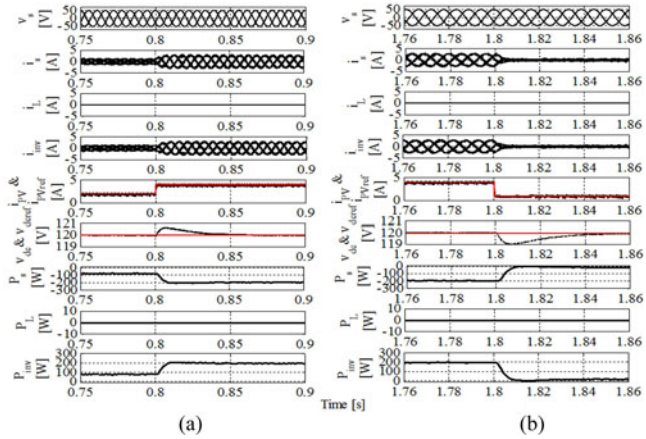

Fig. 9. Dynamic response of the dc/ac inverter under: (a) increasing load and solar irradiation, and (b) decreasing load and solar irradiation.

A. Performance Under Change in Solar Irradiation

Fig. 9 shows simulated results obtained in terms of grid voltage v_s, grid currents i_s, load currents i_L, inverter currents $i_{\rm inv}$, PV current $i_{\rm pvref}$ and $i_{\rm pv}$, dc voltage $v_{\rm dcref}$ and $v_{\rm dc}$, grid power P_s, load power P_L, and inverter power $P_{\rm inv}$. The load demand is negligible under the case.

It is observed in Fig. 9(a) that at 0.8 s, solar irradiation is increased and it results in an increase in $i_{\rm pv}$ and i_s. The dc-bus voltage is well regulated. Due to the absence of any load demand, the power provided by the PV array is equal to that injected to the grid. In Fig. 9(b), the system is subjected to sudden decrease of the solar irradiation at 1.8 s, and it is observed that $i_{\rm pv}$ and i_s are decreased. It is noted that even under reduction in solar-PV power, the dc voltage is well regulated and the steady-state error is negligible and the PV current follows its reference. It confirms the robustness of the control algorithms used for the dc–dc boost converter and dc–ac inverter in steady-state and dynamic conditions.

B. Performance Under Change in Nonlinear Loads

Fig. 10 shows simulation results under load perturbations at constant solar irradiation. Three-phase diode bridge rectifier-feeding resistive-inductive load is considered as the nonlinear

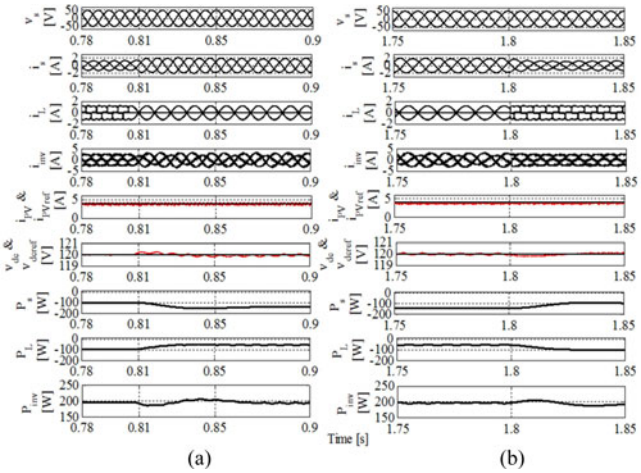

Fig. 10. Dynamic response of the dc/ac inverter under nonlinear loads: (a) fixed solar irradiation and switching off load on phase "a" at $t = 0.81$ s and (b) fixed solar irradiation and switching on load on phase "a" at $t = 1.8$ s.

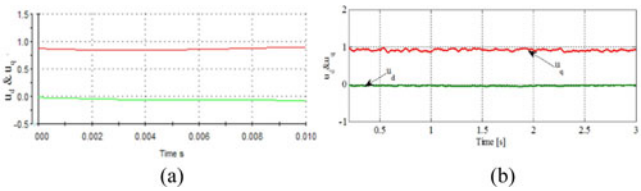

Fig. 11. u_{nd} and u_{nq} obtained at: (a) experimental result and (b) simulation result.

load. Three-phase loads are unbalanced between 0.8 and 1.8 s. It is observed in Fig. 10(a) that until 0.78 s balanced nonlinear load is connected at the PCC and at 0.8 s, the load on phase "b" is switched off. The grid currents are perfectly balanced and sinusoidal. The inverter serves the functions of load balancer and harmonics compensator and injects the active power generated by the PV array in to the grid. In Fig. 10(b), simulation results during switching in load of phase "b" again at 1.8 s are presented. It is observed that the active power injected in to grid is decreased after 1.8 s due to an increase in load demand.

Fig. 11 shows the control laws (u_{nd}) and (u_{nq}), which are obtained using experimental test (a), and that obtained using simulation under identical operating conditions (b).

It is observed that the obtained simulation and experimental results are the same, confirming the validation of the proposed control approach for the dc–ac inverter.

Fig. 12(a) shows the real-time steady-state snapshots of response obtained in terms of three-phase grid voltages v_{sabc}, grid currents i_{sabc}, and load currents i_{Labc}. In Fig. 12(b), the results are obtained for a typical phase "a" variables and dc-link voltage. It is observed that even in the presence of balanced nonlinear loads, the grid voltages and currents are balanced and sinusoidal. To achieve faster convergence and an improved THD, the constant β is selected equal to 5. However, smaller β values can contribute to improve the steady-state performance but they affect the dynamic response of the developed controller.

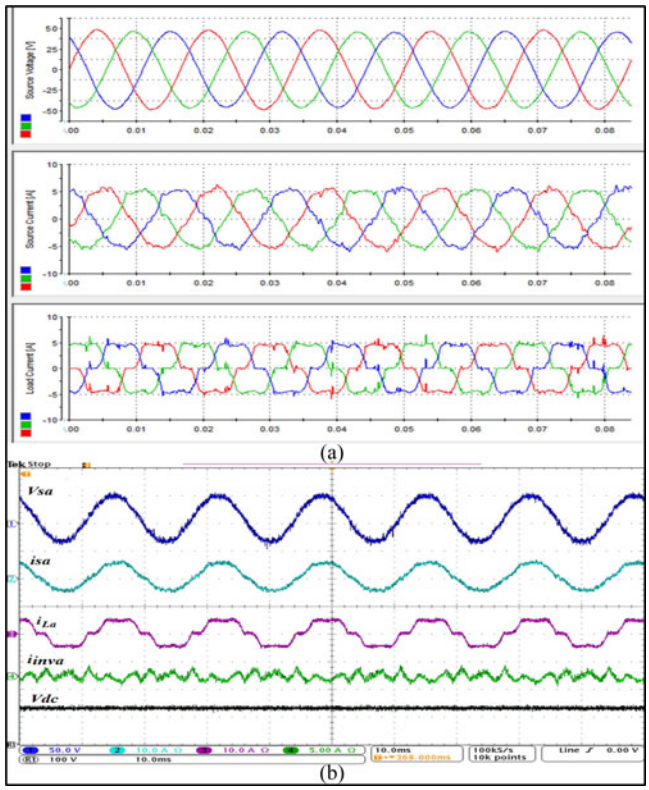

Fig. 12. (a) Three-phase real-time steady-state snapshot at grid side in the presence of balanced nonlinear loads. (b) Oscilloscope results of one phase.

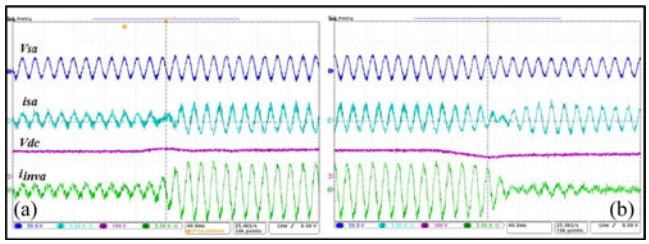

Fig. 13. Dynamic response of the dc/ac inverter under (a) sudden increasing of solar irradiation, and (b) sudden decreasing of solar irradiation at fixed nonlinear load.

Fig. 13(a) and (b) presents experimental results in terms of grid voltage v_{sa}, grid current i_{sa}, dc-link voltage v_{dc}, and inverter current i_{inva} under rise and fall of solar irradiations at fixed nonlinear loads. It is observed in Fig. 13(a) that when solar irradiation is increased at $t = 0.2$ s, grid current is increased and is in out of phase with grid voltage, which leads that the PV array is injecting power to the grid. However, in Fig. 13(b) when solar irradiation decreases at $t = 0.2$ s, grid current becomes in phase with grid voltage. In this case, grid is supplying deficit load demands.

Fig. 14 shows the real-time snapshots of response in terms of three-phase grid voltages v_{sabc}, grid currents i_{sabc}, and load currents i_{Labc} in the presence of unbalanced and balanced nonlinear loads during the absence of the solar irradiation. It is observed

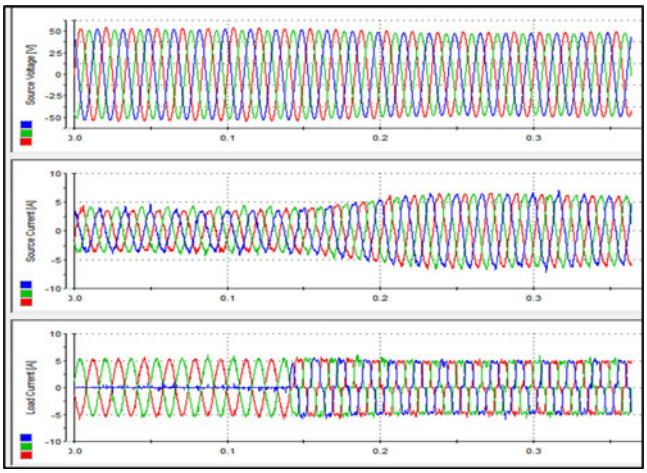

Fig. 14. Three phases real-time steady-state response of the dc/ac inverter in the presence of unbalanced nonlinear loads and absence of solar irradiation.

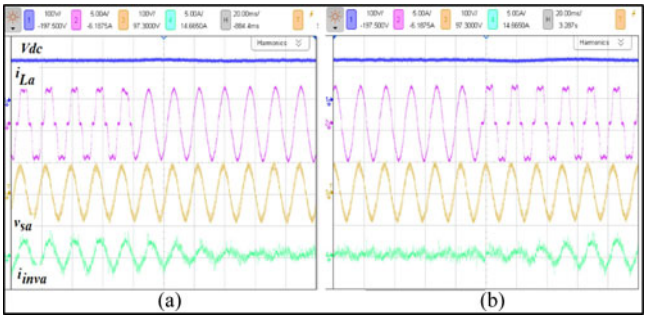

Fig. 15. Test results of the dc voltage, load current, grid voltage, and inverter current in the presence of balanced and unbalanced nonlinear load and at fixed solar irradiation.

that the grid currents and voltages are completely balanced and sinusoidal, which confirms the robustness of the proposed approach based on Lyapunov function for PQ improvement at the PCC.

Fig. 15(a) and (b) shows zoomed view of test results recorded under balanced/unbalanced nonlinear load with constant solar irradiation. It is found that the system is stable and the dc–ac inverter behaves as a shunt active filter. It compensates load current harmonics and provides balanced grid currents under unbalanced nonlinear loads. In addition, the dc voltage is also regulated at its reference value.

Fig. 16(a) shows test results in terms of $v_{\rm dc}$, $i_{\rm pv}$, $v_{\rm sa}$, and $i_{\rm sa}$ during increasing in solar irradiation under no-load conditions. Fig. 16(b) shows results during decreasing in solar irradiation under similar conditions. In Fig. 16(c), it shows zoomed waveforms. It is found that the PV current changes under variation of the solar irradiation and subsequent changes are noticed in grid current. It employs the robustness of the proposed control for the dc–dc boost converter. It is clear that the dynamic response in terms of regulation the dc voltage is fast during the transient period (increasing and decreasing of the solar irradiation).

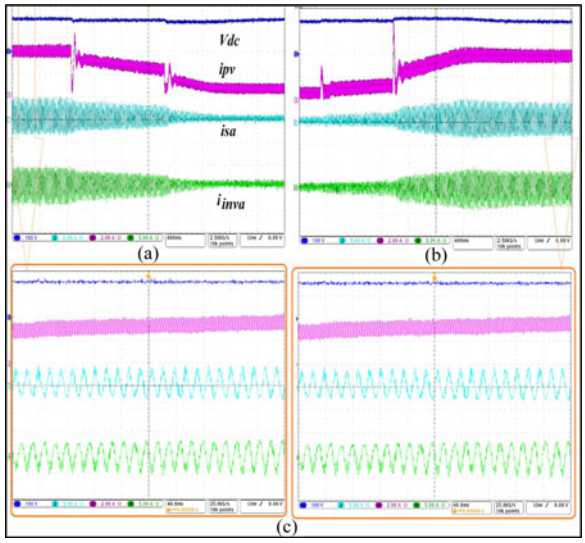

Fig. 16. Experimental results of the dc voltage, output PV current, grid current, and inverter current during solar irradiation change at no load.

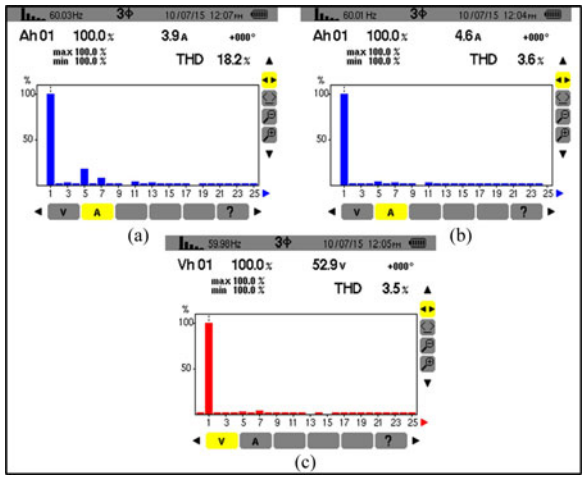

Fig. 17. Harmonics spectra of (a) load current, (b) grid current, and (c) grid voltage.

Fig. 17(a), (b), and (c) presents harmonic spectra and THDs of the load current, grid current, and grid voltage for phase "a," respectively. These THDs of grid current and voltage are within acceptable standard limits of 5% when the load current THD is 18.2%. It clearly demonstrates that the proposed control algorithm serves the function of a harmonics eliminator.

V. Conclusion

A sliding mode and Lyapunov function-based control algorithms were presented for the boost converter and dc–ac inverter used for the solar-PV power-generating system array tied with the grid. Detailed design and stability analysis for both control approaches were discussed to confirm its applicability under various operating conditions. The proposed approach minimized the requirements of a PI controller and only single PI controller was employed for dc-bus voltage loop. The obtained

simulation and experimental results established that presented control approach performed satisfactorily under different operating conditions without adjusting the controller parameters.

APPENDIX

TABLE II
SYSTEM FOR MAGNETIC PARAMETERS

Parameters	Value	Parameters	Value
i_{rr}	$5.981{\cdot}10^{-8}$ A	f_{sw}	10 kHz
i_{scr}	3.81 A	L_f	5 mH
k_i	0.0024	R_f	0.025 Ω
T_r	298 K	k	50
q	$1.6{\cdot}10^{-19}$ C	β	5
k_b	$1.38{\cdot}10^{-23}$ J/K	k_p	0.98
E_g	1.12 V	k_i	200
A	1.2	C_{pv}	100 μF
L	1.5 mH	f	60 Hz
C_{out}	200 μF	v_{Lmax}	50 V
R_c	2.5 Ω	v_{dc}	120 V
C_c	10 μF	C_{dc}	2500 μF

REFERENCES

[1] F. Wu, B. Sun, J. Duan, and K. Zhao, "Online variable topology-type photovoltaic grid-connected inverter," *IEEE Trans. Ind. Electron.*, vol. 62, no. 4, pp. 4814–4822, Aug. 2015.

[2] *IEEE Recommended Practice for Establishing Methods and Procedures That Provide Supplemental Support for Implementation Strategies*, IEEE Std 1547-2014, 2014, pp. 1–176.

[3] H. M. Hasanien, "An adaptive control strategy for low voltage ride through capability enhancement of grid-connected photovoltaic power plants," *IEEE Trans. Power Syst.*, vol. 31, no. 4, pp. 3230–3237, Jul. 2016.

[4] S. Jain and V. Agarwal, "A single-stage grid connected inverter topology for solar PV systems with maximum power point tracking," *IEEE Trans. Power Electron.*, vol. 22, no. 5, pp. 1928–1940, Sep. 2007.

[5] C. Meza, D. Biel, D. Jeltsema, and J. M. A. Scherpen, "Lyapunov-based control scheme for single-phase grid-connected PV central inverters," *IEEE Trans. Control Syst. Technol.*, vol. 20, no. 2, pp. 520–529, Mar. 2012.

[6] S. A. Arshadi, B. Poorali, E. Adib, and H. Farzanehfard, "High step-up DC-AC inverter suitable for AC module applications," *IEEE Trans. Ind. Electron.*, vol. 63, no. 2, pp. 832–839, Feb. 2016.

[7] M. Mirhosseini, J. Pou, and V. G. Agelidis, "Single- and two-stage inverter-based grid-connected photovoltaic power plants with ride-through capability under grid faults," *IEEE Trans. Sustain. Energy*, vol. 6, no. 3, pp. 1150–1159, Jul. 2015.

[8] M. Rezkallah, A. Hamadi, A. Chandra, and B. Singh, "Real-time HIL implementation of sliding mode control for standalone system based on PV array without using dumpload," *IEEE Trans. Sustain. Energy*, vol. 6, no. 4, pp. 1389–1398, Oct. 2015.

[9] Y. Zhu, J. Yao, and D. Wu, "Comparative study of two stages and single stage topologies for grid-tie photovoltaic generation by PSCAD/EMTDC," in *Proc. Int. Conf. Adv. Power Syst. Autom. Protection*, Beijing, China, 2011, pp. 1304–1309.

[10] B. Subudhi and R. Pradhan, "A comparative study on maximum power point tracking techniques for photovoltaic power systems," *IEEE Trans. Sustain. Energy*, vol. 4, no. 1, pp. 89–98, Jan. 2013.

[11] N. Femia, G. Petrone, G. Spagnuolo, and M. Vitelli, "Optimization of perturb and observe maximum power point tracking method," *IEEE Trans. Power Electron.*, vol. 20, no. 4, pp. 963–973, Jul. 2005.

[12] D. Shmilovitz, "On the control of photovoltaic maximum power point tracker via output parameters," *IET Elect. Power Appl.*, vol. 152, no. 2, pp. 239–248, Mar. 2005.

[13] Y. Jiang, J. A. A. Qahouq, and T. A. Haskew, "Adaptive step size with adaptive-perturbation-frequency digital MPPT controller for a single-sensor photovoltaic solar system," *IEEE Trans. Power Electron.*, vol. 28, no. 2, pp. 3195–3205, Jul. 2013.

[14] J. J. Mor, P. F. Puleston, C. Kunusch, and M. A. Fantova, "Development and implementation of a supervisor strategy and sliding mode control setup for fuel-cell-based hybrid generation systems," *IEEE Trans. Energy Convers.*, vol. 30, no. 1, pp. 218–225, Mar. 2015.

[15] M. Edardar, X. Tan, and H. K. Khalil, "Design and analysis of sliding mode controller under approximate hysteresis compensation," *IEEE Trans. Control Syst. Technol.*, vol. 23, no. 2, pp. 598–608, Mar. 2015.

[16] M.-S. Chen, Y.-R. Hwang, and M. Tomizuka, "A state-dependent boundary layer design for sliding mode control," *IEEE Trans. Autom. Control*, vol. 47, no. 10, pp. 1677–1681, Oct. 2002.

[17] A. Ferreira, F. J. Bejarano, and L. M. Fridman, "Robust control with exact uncertainties compensation: With or without chattering?" *IEEE Trans. Control Syst. Technol.*, vol. 19, no. 5, pp. 969–975, Sep. 2011.

[18] P. Liutanakul, S. Pierfederici, and F. Meibody-Tabar, "Application of SMC with I/O feedback linearization to the control of the cascade controlled-rectifier/inverter-motor drive system with small dc-link capacitor," *IEEE Trans. Power Electron.*, vol. 23, no. 5, pp. 2489–2499, Sep. 2008.

[19] C. C. Chen, S. S. D. Xu, and Y. W. Liang, "Study of nonlinear integral sliding mode fault-tolerant control," *IEEE/ASME Trans. Mechatronics*, vol. 21, no. 2, pp. 1160–1168, Apr. 2016.

[20] Q. Xu, "Digital integral terminal sliding mode predictive control of piezoelectric-driven motion system," *IEEE Trans. Ind. Electron.*, vol. 63, no. 6, pp. 3976–3984, Jun. 2016.

[21] A. M. Shotorbani, A. Ajami, S. G. Zadeh, M. P. Aghababa, and B. Mahboubi, "Robust terminal sliding mode power flow controller using unified power flow controller with adaptive observer and local measurement," *IET Gener. Transm. Distrib.*, vol. 8, no. 10, pp. 1712–1723, Oct. 2014.

[22] R. J. Wai, Y. F. Lin, and Y. K. Liu, "Design of adaptive fuzzy-neural-network control for a single-stage boost inverter," *IEEE Trans. Power Electron.*, vol. 30, no. 12, pp. 7282–7298, Dec. 2015.

[23] H. Komurcugil, "Adaptive terminal sliding-mode control strategy for DC-DC buck converters," *ISA Trans.*, vol. 51, no. 6, pp. 673–81, Nov. 2012.

[24] S. C. Tan, Y. M. Lai, and C. K. Tse, "General design issues of sliding-mode controllers in DC-DC converters," *IEEE Trans. Ind. Electron.*, vol. 55, no. 3, pp. 1160–1174, Mar. 2008.

[25] D. G. Montoya, C. A. Ramos-Paja, and R. Giral, "Improved design of sliding-mode controllers based on the requirements of MPPT techniques," *IEEE Trans. Power Electron.*, vol. 31, no. 1, pp. 235–247, Jan. 2016.

[26] M. P. Akter, S. Mekhilef, N. M. L. Tan, and H. Akagi, "Modified model predictive control of a bidirectional AC-DC converter based on Lyapunov function for energy storage systems," *IEEE Trans. Ind. Electron.*, vol. 63, no. 2, pp. 704–715, Feb. 2016.

[27] S. Adhikari, F. Li, and H. Li, "P-Q and P-V control of photovoltaic generators in distribution systems," *IEEE Trans. Smart Grid*, vol. 6, no. 6, pp. 2929–2941, Nov. 2015.

[28] J. W. Jung, N. T. T. Vu, D. Q. Dang, T. D. Do, Y. S. Choi, and H. H. Choi, "A three-phase inverter for a standalone distributed generation system: Adaptive voltage control design and stability analysis," *IEEE Trans. Energy Convers.*, vol. 29, no. 1, pp. 46–56, Mar. 2014.

[29] S. Rahmani, A. Hamadi, and K. Al-Haddad, "A Lyapunov-function-based control for a three-phase shunt hybrid active filter," *IEEE Trans. Ind. Electron.*, vol. 59, no. 3, pp. 1418–1429, Mar. 2012.

[30] H. Komurcugil, N. Altin, S. Ozdemir, and I. Sefa, "An extended Lyapunov-function-based control strategy for single-phase UPS inverters," *IEEE Trans. Power Electron.*, vol. 30, no. 7, pp. 3976–3983, Jul. 2015.

[31] B. Singh, A. Chandra, and K. Al-Haddad, *Power Quality Problems And Mitigation Techniques*, 1st ed. Chichester, U.K.: Wiley, 2015, pp. 132–133.

Miloud Rezkallah (S'11–M'14) received the B.Tech. degree in electrical machines and drives from the University of Science and Technology (now University Mohamed Boudiaf), Oran, Algeria, in 1998, and the M.Tech. and Ph.D. degrees in power electronics and system control from the École de Technologie Supérieure, Université du Québec, Montréal, QC, Canada, in 2010 and 2016, respectively.

He is a Postdoctoral Research Fellow in the Electrical Engineering Department, École de Technologie Supérieure. His research interests include control and design of microgrids, active filters, renewable energy generation and applications, and energy storage systems.

Shailendra Kumar Sharma (S'09–M'12–SM'15) received the M.E. degree from Shri Govindram Seksaria Institute of Technology and Science, Indore, India, in 2004, and the Ph.D. degree from the Indian Institute of Technology Delhi, New Delhi, India, in 2012, both in electrical engineering.

He was an Erection and Commissioning Engineer with textile and power industries during 1995–2002. Since 2004, he has been an Assistant Professor in the Electrical Engineering Department, Shri Govindram Seksaria Institute of Technology and Science. He was a Postdoctoral Research Fellow during 2015–2016 in the Electrical Engineering Department, École de Technologie Supérieure, Université du Québec, Montréal, QC, Canada. His main research interests include control of stand-alone nonconventional energy sources, distributed energy resources with grid, power quality, and special machine drives.

Dr. Sharma is an Associate Member of the Institution of Engineers, India.

Ambrish Chandra (SM'99–F'14) received the B.Ing. degree in electrical engineering from the Indian Institute of Technology (IIT), Roorkee, India, in 1977, the M.Tech. degree in power apparatus and systems from the IIT, New Delhi, India, in 1980, and the Ph.D. degree in electrical engeneering from the University of Calgary, Calgary, AB, Canada, in 1987.

From 2012 to 2015, he was the Director of the graduate program on "renewable energy and energy efficiency" at the École de Technologie Supérieure, Université du Québec, Montréal, QC, Canada, where since 1994, he has been a Professor in the Department of Electrical Engineering. He coauthored the book *Power Quality—Problems and Mitigation Techniques* (Wiley, 2015). His research interests include power quality, active filters, static reactive power compensation, flexible ac transmission systems, and control and integration of renewable energy resources.

Prof. Chandra is a Distinguished Lecturer of the IEEE Power and Energy Society and also of the IEEE Industry Applications Society. He is an Associate Editor of the IEEE TRANSACTIONS ON INDUSTRIAL ELECTRONICS. He is a Professional Engineer in the Province of Quebec, Canada.

Bhim Singh (SM'99–F'10) was born in Rahamapur, India, in 1956. He received the B.E. degree from the University of Roorkee, Roorkee, India, in 1977, and the M.Tech. and Ph.D. degrees from the Indian Institute of Technology Delhi (IIT Delhi), New Delhi, India, in 1979 and 1983, respectively, all in electrical engineering.

In 1983, he joined the Department of Electrical Engineering, University of Roorkee, as a Lecturer. He became a Reader there in 1988. In December 1990, he joined the Department of Electrical Engineering, IIT Delhi, as an Assistant Professor, where he became a Professor in 1997. He is currently the Head of the Department of Electrical Engineering, IIT Delhi. He has guided 60 Ph.D. dissertations, 161 M.E./M.Tech./M.S.(R) theses. His research interests include power electronics, electrical machines and drives, renewable energy, active filters, flexible ac transmission systems, high-voltage direct current, and power quality.

Daniel R. Rousse has studied philosophy and literature. He received the B.Eng. and Master's degrees from the Ecole Polytechnique de Montréal, Université de Montréal, Montréal, QC, USA, in 1985 and 1988, respectively, and the Ph.D. degree from McGill University, Montréal, in 1994, all in mechanical engineering.

He is a Full Professor at the École de Technologie Supérieure, Montréal, where he is the Director of the t3e Group and the Director of the Master's program in renewable energy and energy efficiency. He was a Professor of energy with Laval University (1995) before accepting the position of Vice President for Development – Lévis campus at the Université du Québec in Rimouski (2004) to build an energy efficient 15 000 m^2 campus involving a geothermal field of 125 boreholes, an enthalpy wheel, passive solar shields, active solar walls, etc. From 2007 to 2009, he was the Director of development and special projects of the network of the University du Quebec, in charge of the Energy Workshop involving four universities. His technologies research activities in energy and energy efficiency are focused on three main areas: solar, storage, and sustainable buildings.